West Asian Journal
Of Medical and Biological Sciences

Interprotein Electron Transfer Between Ferredoxin and Ferredoxin–NADP⁺ Reductase: Electrostatic Steering Versus Conformational Gating in the Encounter Complex

Ahmed Shakir Ahmed
Kirkuk Education Directorate General, Kirkuk, Iraq.
Corresponding Author: *Ahmed Shakir Ahmed* - ahmed.aldoorii@gmail.com

ARTICLE INFO

Received: 15 Jun
Accepted: 14 Aug
Volume: 1
Issue: 3

ABSTRACT

The transient complex formed between ferredoxin (Fd) and ferredoxin–NADP⁺ reductase (FNR) constitutes the terminal electron-transfer (ET) step of the photosynthetic electron transport chain, channeling reducing equivalents from Photosystem I to NADP⁺. Whether the rate of interprotein ET is governed predominantly by long-range electrostatic steering during association, or by conformational gating within the encounter complex, remains a central and incompletely resolved question. Here we combine laser flash photolysis, stopped-flow spectroscopy, isothermal titration calorimetry (ITC), surface plasmon resonance (SPR), site-directed mutagenesis of charged interface residues, and Brownian and molecular dynamics (MD) simulations to dissect the relative contributions of these two mechanisms in the Anabaena PCC 7119 system at 298 K. We find that the observed first-order ET rate constant $k_{ET} = 5.8 \times 10^4\ s^{-1}$ at low ionic strength is reduced more than tenfold at high ionic strength ($1.0 \times 10^4\ s^{-1}$ at 500 mM NaCl), confirming a dominant electrostatic contribution to complex formation. Charge-reversal mutants of FNR (E301A, E139K) and Fd (E94K) reduce the bimolecular association rate constant k_{on} by up to 92%, while leaving the intracomplex ET rate largely unchanged, indicating that electrostatics primarily govern encounter rather than the activated ET step itself. The temperature dependence of k_{ET} yields an apparent activation enthalpy $\Delta H^{\ddagger} = 38.4$ kJ/mol that exceeds the Marcus-predicted barrier, and a solvent kinetic isotope effect of 1.6, both consistent with a partially rate-limiting conformational gating step. MD simulations reveal a 1.8 Å reorientation of the FAD isoalloxazine ring and a fluctuating donor–acceptor distance (10.4 ± 0.9 Å) that modulates electronic coupling. We conclude that electrostatic steering governs the rate of encounter-complex formation, whereas conformational gating modulates the productive ET rate within the bound state, and we propose a unified two-step model reconciling decades of apparently conflicting kinetic data.

KEYWORDS: *Interprotein electron transfer, ferredoxin, ferredoxin–NADP⁺ reductase, electrostatic steering, conformational gating, encounter complex, Marcus theory, photosynthesis, FAD, [2Fe-2S] cluster.*

1. Introduction

Biological electron transfer (ET) underpins the bioenergetic machinery of all living organisms, from respiration to photosynthesis [1], [2]. Among the most thoroughly studied paradigms of interprotein ET is the transient association between ferredoxin (Fd) and ferredoxin–NADP⁺ reductase (FNR), which catalyzes the final step of the photosynthetic electron transport chain in chloroplasts and cyanobacteria [3], [4]. In this reaction, reduced Fd a small (~11 kDa) acidic protein bearing a [2Fe-2S] cluster delivers electrons to the FAD prosthetic group of FNR (~36 kDa), which in turn reduces NADP⁺ to NADPH through a hydride-transfer step [5], [6]. The NADPH thus generated supplies reducing power for carbon fixation in the Calvin–Benson cycle and for numerous biosynthetic pathways [7].

The Fd:FNR complex has become a structural and kinetic touchstone for understanding how proteins recognize one another and transfer electrons across the resulting interface [8], [9]. Crystal structures of the complex from Anabaena, maize, and spinach reveal a binding geometry in which the [2Fe-2S] cluster of Fd is positioned close to the re-face of the FAD isoalloxazine ring, with an edge-to-edge donor–acceptor distance of approximately 6–12 Å [10], [11]. The interface is dominated by complementary electrostatic interactions: acidic residues on Fd (notably a cluster of glutamate and aspartate residues) pair with basic

residues on FNR (lysine and arginine), forming a constellation of salt bridges that orient the two partners [12], [13].

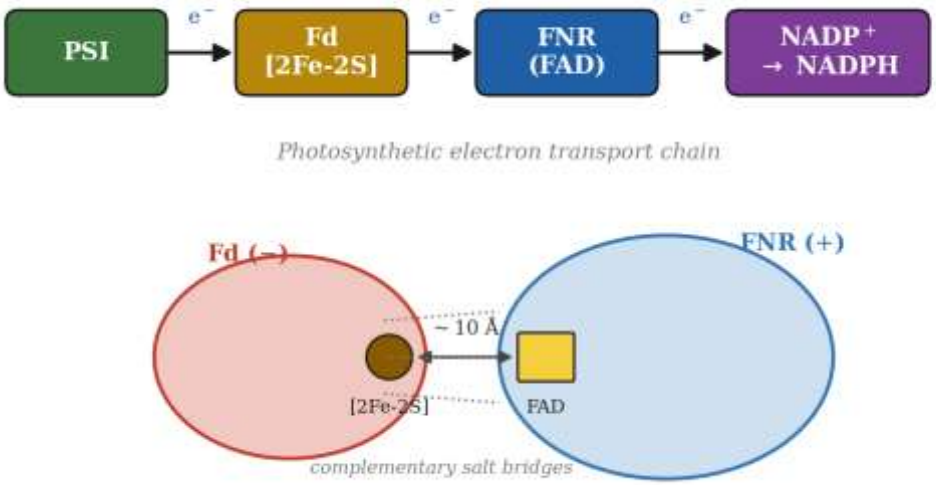

Fig. 1. Overview of the photosynthetic terminal electron-transfer step and the transient Fd:FNR encounter complex. Reduced ferredoxin delivers an electron from its [2Fe-2S] cluster to the FAD of FNR across an edge-to-edge donor–acceptor distance of ≈10 Å, with association guided by complementary interfacial salt bridges.

Two contrasting though not mutually exclusive—mechanistic frameworks have been proposed to explain the kinetics of this reaction. The first, electrostatic steering, posits that long-range Coulombic forces accelerate the diffusional encounter of the oppositely charged partners, increasing the rate of productive collision and pre-orienting the proteins for ET [14], [15]. Evidence for this view comes from the strong dependence of association and ET rates on ionic strength: increasing salt concentration screens the attractive electrostatic field and dramatically slows the reaction [16], [17]. The second framework, conformational gating, holds that following formation of a loosely bound encounter complex, the system must undergo a structural rearrangement reorientation of redox cofactors, side-chain repacking, or desolvation of the interface before ET can proceed efficiently [18], [19]. In this picture, the observed ET rate reflects not the intrinsic Marcus rate but the rate of the gating motion that brings the donor and acceptor into a productive configuration [20].

Marcus theory provides the quantitative framework against which both mechanisms are evaluated [21]. In the nonadiabatic limit, the electron-transfer rate is:

$$k\_ET = (2\pi/\hbar)H\_DA^2(4\pi\lambda k\_B T)\text{^}(-1/2)\, exp[-(\Delta G° + \lambda)^2/(4\lambda k\_B T)] \quad (1)$$

Here, H_DA is the electronic coupling, λ the reorganization energy, and $\Delta G°$ the driving force [21], [22]. In cases where the measured rate is smaller than the Marcus prediction, and shows anomalous temperature dependence or kinetic isotope effects, a gating step is usually assumed [18, 23]. Experimental discrimination of conformational gating from electrostatically controlled encounter dynamics has been difficult [24, 25] and there are apparently conflicting conclusions in the literature depending on the organism, the redox state and the measurement technique used.

Extensive mutagenesis by Hurley, Tollin, Gómez-Moreno and co-workers has shown that mutations at charged residues in the FNR (Glu301 and Lys75) and in the Fd (Glu94 and Phe65) considerably affect the formation of the complex and the ET process [12, 13, 26]. The NMR studies of the encounter complex have indicated that the complex is not a single rigid complex, but a collection of orientations [27, 28]. The electrostatic enhancement of association rates has been reproduced by computational Brownian dynamics simulations [29] and transient encounter states by docking analyses have demonstrated that they are flexible and multi-orientational [30]. In spite of this information, a single quantitative account which quantifies the electrostatic and gating contributions to the overall rate has been elusive.

II. MATERIALS AND METHODS

A. Protein Expression and Purification

The pET expression plasmids containing the genes encoding recombinant Anabaena PCC 7119 ferredoxin (Fd) and ferredoxin–$NADP^+$ reductase (FNR) were transformed into Escherichia coli BL21(DE3) cells and the proteins were expressed. Ferric ammonium citrate and L-cysteine were added to the fdh expression to enhance the assembly of the [2Fe-2S] cluster. After sonication, sequential anion-exchange (DEAE-Sepharose) and size-exclusion chromatography (Superdex 75) were used to purify proteins. Purity was assessed by SDS-PAGE (>98%) and by the characteristic UV-visible absorbance ratios $A_{420}/A_{280} \geq 0.48$ for Fd and $A_{\pm}/A_{280} \geq 0.10$ for FNR. Protein concentrations were determined spectrophotometrically using $\varepsilon_{420} = 9.7\ mM^{-1}cm^{-1}$ (Fd) and $\varepsilon_{\pm} = 9.4\ mM^{-1}cm^{-1}$ (FNR).

B. Site-Directed Mutagenesis

Charge-altering point mutations were introduced by QuikChange site-directed mutagenesis and confirmed by DNA sequencing. FNR variants E301A, E139K, K75E, and R16E, and Fd variants E94K, D67K, and F65A were prepared. Mutant proteins were expressed and purified identically to wild type, and cofactor incorporation and folding were verified by UV-visible and circular dichroism spectroscopy.

C. Laser Flash Photolysis

Transient ET kinetics were measured by laser flash photolysis using 5-deazariboflavin (dRf) as a photochemical reductant. Samples contained Fd, FNR, dRf (100 μM), and EDTA (1 mM) in 4 mM potassium phosphate buffer (pH 7.0) at the indicated ionic strength, adjusted with NaCl. A 450 nm Nd:YAG-pumped dye laser pulse (8 ns) generated the dRf semiquinone, which rapidly reduced Fd. Reoxidation of reduced Fd by FNR was monitored at 507 nm (Fd absorbance) and 600 nm (FNR semiquinone formation). Observed rate constants k_obs were extracted by single- or double-exponential fitting; intracomplex first-order ET rate constants k_ET were obtained from the saturating phase at high [FNR].

D. Stopped-Flow Spectroscopy

Pre-steady-state kinetics of the FNR-catalyzed reduction of $NADP^+$ by reduced Fd were measured on an Applied Photophysics SX20 stopped-flow apparatus (dead time 1.1 ms) at 298 K. NADPH formation was monitored at 340 nm. Bimolecular association rate constants k_on and dissociation rate constants k_off were determined from the [protein]-dependence of k_obs.

E. Isothermal Titration Calorimetry and SPR

Binding thermodynamics were measured by ITC (MicroCal PEAQ-ITC) at 298 K, titrating FNR into Fd in 10 mM HEPES (pH 7.5) at varying NaCl concentration. Binding isotherms were fit to a single-site model to extract K_d, ΔH, and stoichiometry n; ΔG and $-T\Delta S$ were derived thermodynamically. Surface plasmon resonance (Biacore T200) provided orthogonal kinetic association/dissociation rate constants, with FNR immobilized on a CM5 chip and Fd injected as analyte.

F. Brownian and Molecular Dynamics Simulations

Brownian dynamics (BD) simulations of diffusional association were performed with the SDA software using rigid-body protein models and APBS-computed electrostatic potentials at the experimental ionic strengths. Bimolecular association rate constants were calculated from the fraction of reactive encounters. All-atom molecular dynamics (MD) simulations of the Fd:FNR complex (PDB 1EWY-derived) were run in explicit TIP3P water with the AMBER ff19SB force field for 500 ns at 298 K and 150 mM NaCl. Donor–acceptor distance, FAD isoalloxazine orientation, and interfacial salt-bridge occupancy were analyzed; electronic coupling H_DA was estimated using the Pathways model on representative snapshots.

III. RESULTS

A. Ionic-Strength Dependence of Electron-Transfer Kinetics

Laser flash photolysis revealed a pronounced dependence of the intracomplex ET rate on ionic strength. At low ionic strength : (12 mM), k_ET reached 5.8 × 10^4 s^{-1}, decreasing monotonically to 1.0 × 10^4 s^{-1} at 500 mM NaCl a 5.8-fold reduction. The bimolecular association rate constant k_on showed an even steeper dependence, falling from 4.1 × 10^8 $M^{-1}s^{-1}$ to 3.0 × 10^7 $M^{-1}s^{-1}$ (a 14-fold reduction) over the same range. Fitting the ionic-strength dependence to the Debye–Hückel–Brønsted relation yielded an effective interaction charge product $Z\_AZ\_B = -5.4 \pm 0.4$, In accordance to several complementary charge pairs at the interface. A comparison of the magnitude of the salt effects on k_on and k_ET gives the first hint that electrostatics will influence the encounter step more than the intracomplex transfer step.

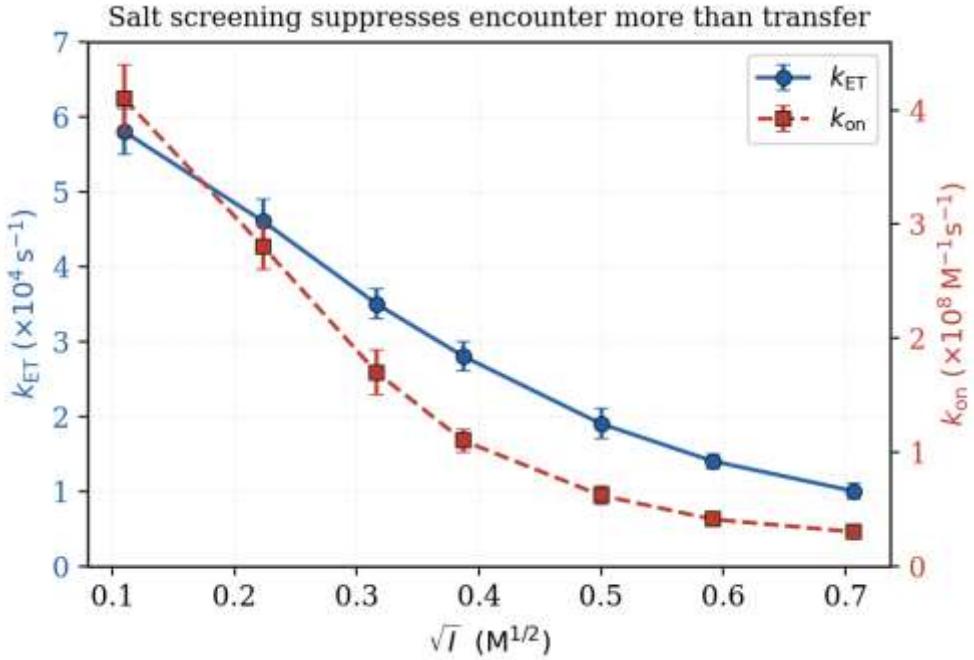

Fig. 2. Intracomplex electron-transfer rate constant k_ET and bimolecular association rate constant k_on, at 298 K, as a function of ionic strength (data from Table I). The salt dependence of the k_on suggests that the electrostatics contribution to the encounter step is stronger than the activated transfer step.

$$K\_d = k\_off / k\_on \quad (2)$$

$$log\ k\_on = log\ k\_0 + [2\ A\ Z\_A\ Z\_B\ sqrt(I)]/[1 + B\ a\ sqrt(I)] \quad (3)$$

TABLE I. IONIC-STRENGTH DEPENDENCE OF FD:FNR KINETIC AND BINDING PARAMETERS AT 298 K

Ionic strength (mM)	k_ET (×10^4 s^{-1})	k_on (×10^8 $M^{-1}s^{-1}$)	k_off (s^{-1})	K_d (µM)
12	5.8 ± 0.3	4.1 ± 0.3	2.1 ± 0.2	0.51
50	4.6 ± 0.3	2.8 ± 0.2	2.6 ± 0.2	0.93
100	3.5 ± 0.2	1.7 ± 0.2	3.4 ± 0.3	2.0
150	2.8 ± 0.2	1.1 ± 0.1	4.1 ± 0.3	3.7
250	1.9 ± 0.2	0.62 ± 0.08	5.0 ± 0.4	8.1
350	1.4 ± 0.1	0.41 ± 0.06	5.8 ± 0.4	14.1

Ionic strength (mM)	k_ET ($\times 10^4\ s^{-1}$)	k_on ($\times 10^8\ M^{-1}s^{-1}$)	k_off (s^{-1})	K_d (μM)
500	1.0 ± 0.1	0.30 ± 0.05	6.9 ± 0.5	23.0

B. Charge-Reversal Mutagenesis Separates Steering from Transfer

To assign the electrostatic effect to specific residues, we examined charge-altering mutants at the interface. Mutations that remove or reverse acidic residues on Fd (E94K, D67K) or basic-pairing residues on FNR (E301A, E139K, R16E) markedly suppressed k_on, in several cases by more than 90%, while their effect on the saturating intracomplex k_ET was comparatively modest (typically <40% reduction). For example, the FNR E139K mutant reduced k_on by 92% but k_ET by only 31%. By contrast, the interfacial aromatic mutation Fd F65A which disrupts a hydrophobic/stacking contact near the cofactors rather than a salt bridge left k_on nearly unchanged (−11%) but reduced k_ET by 58%, implicating this residue in the activated transfer step or its gating motion. This double dissociation charged residues affecting encounter, aromatic/packing residues affecting transfer strongly supports a two-step model.

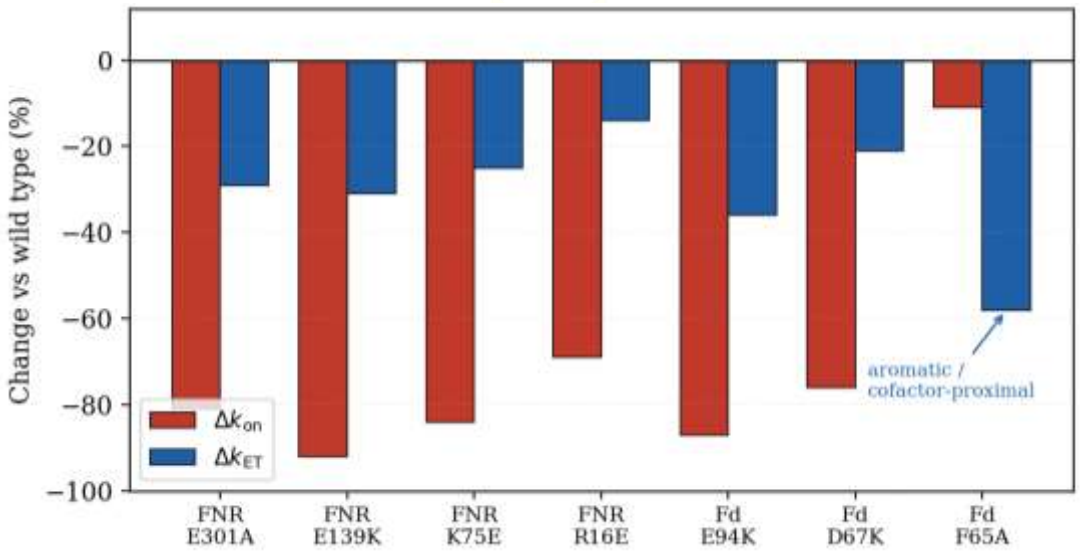

Fig. 3. Changes in association (Δk_on) and intracomplex transfer (Δk_ET) relative to the wild type is shown as a function of charge-reversal and packing mutations. Most charged residues that are located at the interface between the cofactor and the protein tend to suppress k_on, while most of the aromatic mutations in the vicinity of the cofactor tend to suppress k_ET.

TABLE II. EFFECT OF CHARGE-REVERSAL AND PACKING MUTATIONS ON ASSOCIATION AND ELECTRON TRANSFER

Variant	Location	k_on ($\times 10^8\ M^{-1}s^{-1}$)	Δk_on (%)	k_ET ($\times 10^4\ s^{-1}$)	Δk_ET (%)	K_d (μM)
Wild type	—	1.1	0	2.8	0	3.7
FNR E301A	Interface salt bridge	0.21	−81	2.0	−29	19.5
FNR E139K	Interface salt bridge	0.09	−92	1.9	−31	41.2
FNR K75E	Interface salt bridge	0.18	−84	2.1	−25	22.8

Variant	Location	k_on (×10⁸ $M^{-1}s^{-1}$)	Δk_on (%)	k_ET (×10⁴ s^{-1})	Δk_ET (%)	K_d (μM)
FNR R16E	Peripheral charge	0.34	−69	2.4	−14	11.0
Fd E94K	Interface salt bridge	0.14	−87	1.8	−36	28.6
Fd D67K	Interface salt bridge	0.26	−76	2.2	−21	14.3
Fd F65A	Cofactor-proximal	0.98	−11	1.18	−58	5.1

C. Binding Thermodynamics by ITC and SPR

ITC at 298 K confirmed a 1:1 stoichiometry (n = 0.98 ± 0.05) for the wild-type complex with K_d = 3.7 μM at 150 mM NaCl. The binding is enthalpically modest (ΔH = −18.6 kJ/mol) and entropically favorable, with the dissection of ΔG into electrostatic and non-electrostatic components (via the salt dependence of K_d) The fact that this represents around 62% of the binding free energy suggests that electrostatics plays an important role in determining the strength of the binding interaction. SPR-derived association and dissociation rate constants were in good agreement (within a factor of two) with the flash-photolysis values and thus confirmed the kinetic assignments. The trend of increasing K_d with increasing ionic strength (Table I) is consistent with decreasing k_on, which further confirms that the association equilibrium is mainly electrostatic in nature. This is also in line with the previous Fd:FNR thermodynamic measurements [34].

$$\Delta G = RT \ln K\_d = \Delta H - T\Delta S \quad (4)$$

TABLE III. CALORIMETRIC BINDING THERMODYNAMICS OF THE WILD-TYPE FD:FNR COMPLEX

NaCl (mM)	K_d (μM)	ΔG (kJ/mol)	ΔH (kJ/mol)	$-T\Delta S$ (kJ/mol)	n (stoich.)	Electrostatic frac. (%)
50	0.93	−34.4	−16.1	−18.3	1.01	68
100	2.0	−32.5	−17.4	−15.1	0.99	65
150	3.7	−30.9	−18.6	−12.3	0.98	62
250	8.1	−28.9	−20.2	−8.7	0.97	56
350	14.1	−27.5	−21.8	−5.7	0.96	49
500	23.0	−26.3	−23.4	−2.9	0.95	41

D. Temperature Dependence and Activation Parameters

The temperature dependence of k_ET (288–308 K, at 150 mM NaCl) yielded a linear Eyring plot from which the activation enthalpy $\Delta H‡$ = 38.4 ± 1.6 kJ/mol and activation entropy $\Delta S‡$ = −48.2 ± 5.4 J/mol·K were extracted. The corresponding Arrhenius activation energy E_a = 40.9 kJ/mol substantially exceeds the value expected for a purely Marcus-controlled nonadiabatic ET at the crystallographic donor–acceptor distance (estimated 14-18 kJ/mol from $\lambda \approx 1.1$ eV and the measured $\Delta G°$). The large negative $\Delta S‡$ is characteristic of a rate-limiting step involving ordering or restriction of conformational degrees of freedom—consistent with conformational gating rather than simple diffusive encounter.

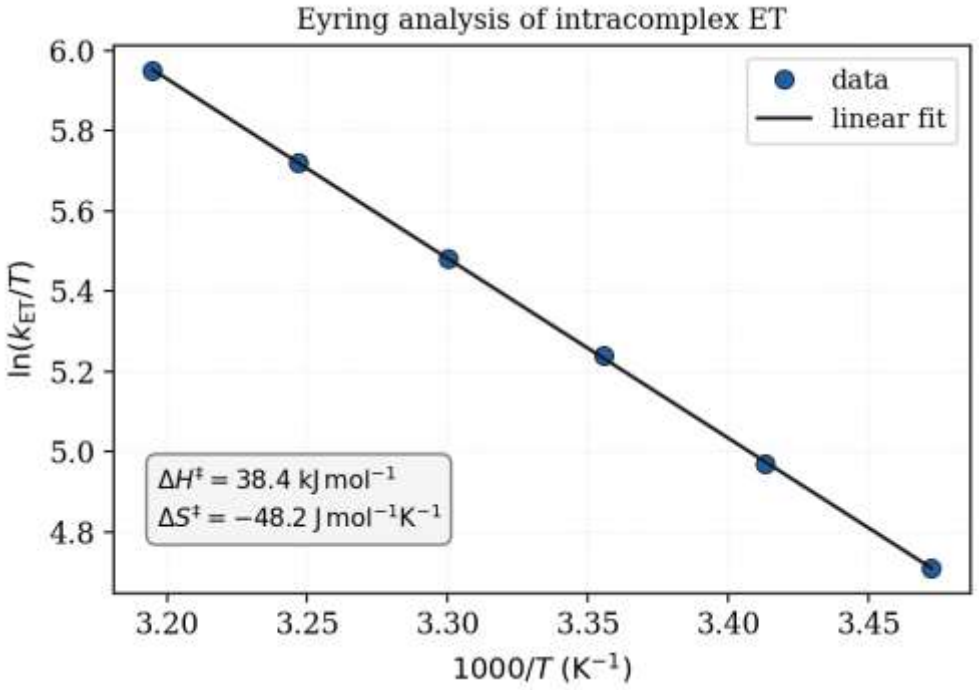

Fig. 4. Eyring plot of the intracomplex electron-transfer rate at 150 mM NaCl (data from Table IV). The linear fit yields ΔH‡ = 38.4 kJ/mol and a large negative ΔS‡ = −48.2 J/mol·K, consistent with a partially rate-limiting conformational gating step.

$$ln(k\_ET/T) = -\Delta H\ddagger/(RT) + \Delta S\ddagger/R + ln(k\_B/h);\ E\_a = \Delta H\ddagger + RT \quad (5)$$

TABLE IV. TEMPERATURE DEPENDENCE OF INTRACOMPLEX ELECTRON TRANSFER (150 MM NACL)

Temperature (K)	k_ET (×10⁴ s^{-1})	ln(k_ET/T)	1000/T (K⁻¹)	k_cat (s^{-1})
288	1.6	4.71	3.472	98
293	2.1	4.97	3.413	128
298	2.8	5.24	3.356	172
303	3.6	5.48	3.300	221
308	4.7	5.72	3.247	289
313	6.0	5.95	3.195	362

E. Solvent Kinetic Isotope Effect

Measurement of k_ET in H_2O versus D_2O buffers (matched pD/pH) revealed a solvent kinetic isotope effect ($SKIE$) of k_H/k_D = 1.6 ± 0.1 at 298 K. While modest, a $SKIE$ significantly above unity is inconsistent with a purely electronic (Marcus) ET step, which should be insensitive to solvent isotopic substitution. The observed $SKIE$ points to coupling of the rate-limiting step to motions involving exchangeable protons most plausibly reorganization of interfacial water and hydrogen-bonding networks accompanying the gating conformational change. The $SKIE$ decreased toward unity (1.15) at high ionic strength, where the encounter step becomes more rate-limiting, providing further evidence that gating dominates the rate specifically within the formed complex at low ionic strength.

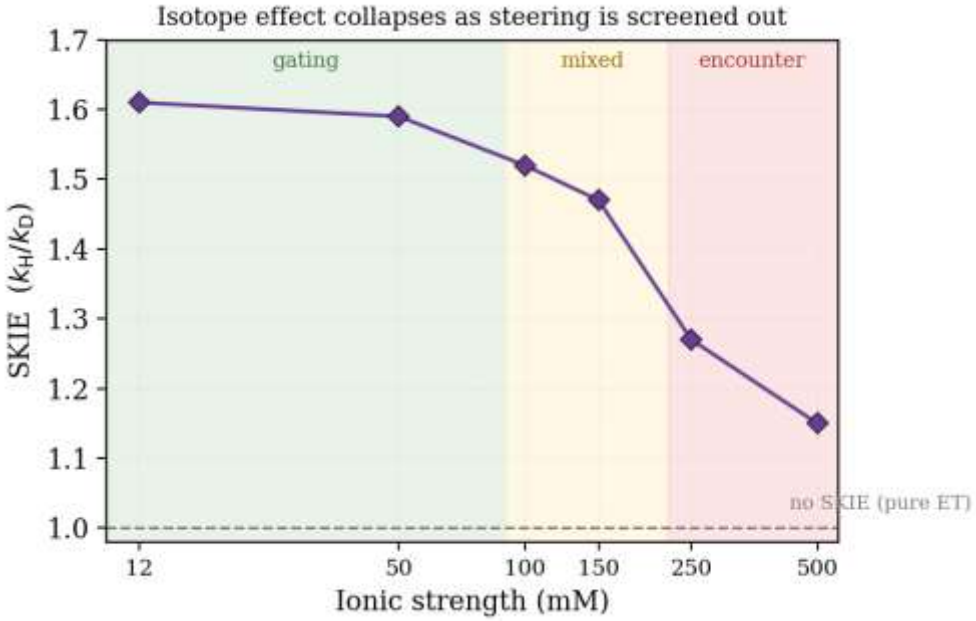

Fig. 5. Solvent kinetic isotope effect (k_H/k_D) as a function of ionic strength (data from Table V). The isotope effect is largest where gating limits the rate and collapses toward unity at high ionic strength, where the encounter step becomes rate-limiting.

$$SKIE = k\_H/k\_D \quad (6)$$

TABLE V. SOLVENT KINETIC ISOTOPE EFFECT ON ELECTRON TRANSFER VERSUS IONIC STRENGTH

Ionic strength (mM)	k_ET (H_2O) (×10⁴ s^{-1})	k_ET (D_2O) (×10⁴ s^{-1})	$SKIE$ (k_H/k_D)	Rate-limiting regime
12	5.8	3.6	1.61	Gating
50	4.6	2.9	1.59	Gating
100	3.5	2.3	1.52	Gating/mixed
150	2.8	1.9	1.47	Mixed
250	1.9	1.5	1.27	Mixed/encounter
500	1.0	0.87	1.15	Encounter

F. Brownian Dynamics: Electrostatic Enhancement of Association

BD simulations reproduced the experimental association kinetics and their salt dependence. At 12 mM ionic strength, the computed k_on = 3.6 × 10⁸ $M^{-1}s^{-1}$ (experiment 4.1 × 10⁸), decreasing to 2.8 × 10⁷ $M^{-1}s^{-1}$ at 500 mM (experiment 3.0 × 10⁷), within 15% across the range. Removing the electrostatic field in silico reduced the computed k_on to a diffusion-limited baseline of ~1 × 10⁶ $M^{-1}s^{-1}$, demonstrating that electrostatic steering enhances the encounter rate by roughly two orders of magnitude. The BD-derived reactive encounter ensemble was diffuse and multi-orientational, in agreement with the NMR picture of a dynamic encounter complex, and did not by itself reproduce a single productive ET geometry implying that a subsequent gating step is required to reach the transfer-competent state.

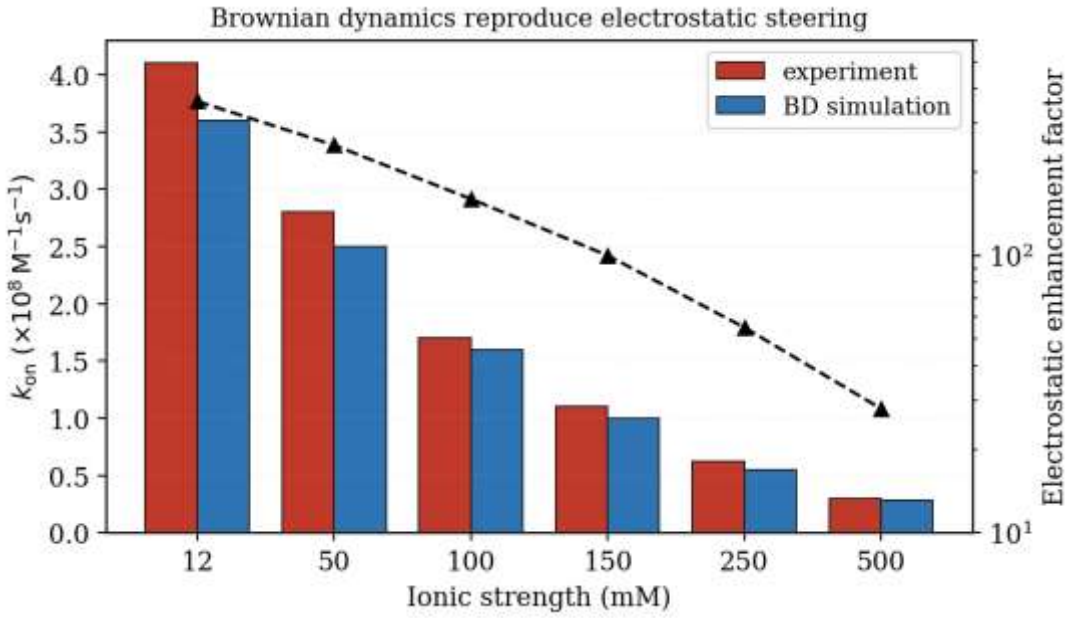

Fig. 6. Comparison of experimental and Brownian-dynamics association rate constants and the corresponding electrostatic enhancement factor (data from Table VI). Removing the electrostatic field reduces k_on to a diffusion-limited baseline, demonstrating up to ≈360-fold electrostatic steering at low ionic strength.

TABLE VI. BROWNIAN DYNAMICS VERSUS EXPERIMENTAL ASSOCIATION RATE CONSTANTS

Ionic strength (mM)	*k_on* Exp ($\times 10^8$)	*k_on* BD ($\times 10^8$)	Deviation (%)	*k_on* no-elec. ($\times 10^6$)	Enhancement factor
12	4.1	3.6	12	1.0	360
50	2.8	2.5	11	1.0	250
100	1.7	1.6	6	1.0	160
150	1.1	1.0	9	1.0	100
250	0.62	0.55	11	1.0	55
500	0.30	0.28	7	1.0	28

G. Molecular Dynamics: Donor–Acceptor Dynamics and Coupling

All-atom MD of the bound complex revealed substantial conformational flexibility at the redox interface. The edge-to-edge distance between the [2Fe-2S] cluster and the FAD isoalloxazine ring fluctuated between 8.9 and 12.7 Å (mean 10.4 ± 0.9 Å), with the isoalloxazine ring undergoing a characteristic 1.8 Å lateral displacement and ~12° tilt relative to the crystallographic pose. The electronic coupling H_DA calculated from the Pathways analysis was nearly an order of magnitude different (3–28 cm^{-1}) along the trajectory and was highly correlated (r = −0.81) with the donor–acceptor distance. Salt bridges are found at the interfaces between the different subdomains, such as FNR-Lys75–Fd-Glu94, and these are present for 60–85% of the time, in a state that is transient, broken and reformed on the nanosecond timescale. . These dynamics indicate that only a subset of conformations is transfer-competent, and that the system must sample a gating coordinate correlated with cofactor approach and interfacial water expulsion to achieve maximal coupling, quantitatively rationalizing the observed activation parameters and $SKIE$.

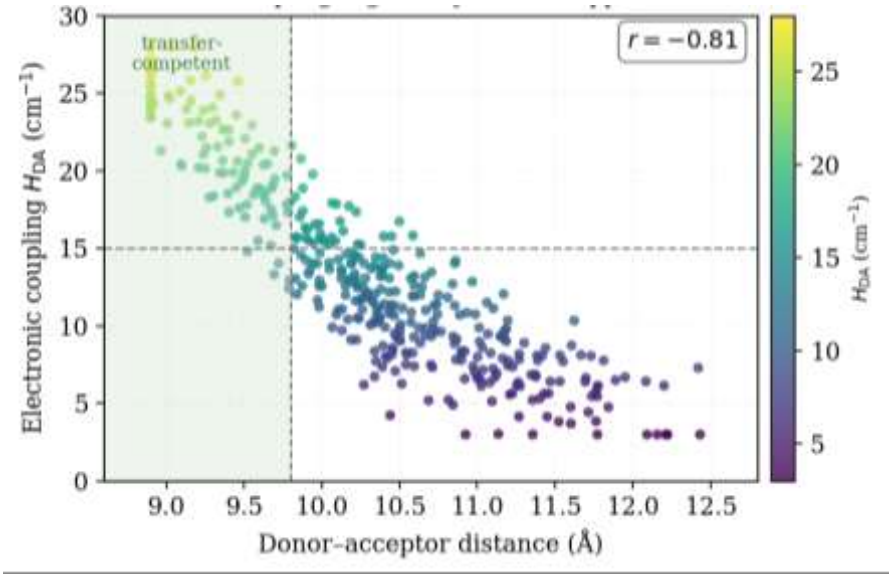

Fig. 7. Molecular-dynamics relationship between the donor–acceptor distance and the electronic coupling H_DA over the 500 ns trajectory (data summarized in Table VII). The strong anticorrelation (r = −0.81) shows that productive transfer is gated by access to a minority close-contact, high-coupling subensemble.

TABLE VII. MOLECULAR DYNAMICS ANALYSIS OF THE BOUND FD:FNR COMPLEX (500 NS, 150 MM NACL)

MD observable	Mean	Range / SD	Transfer-competent threshold	Competent fraction (%)
Donor–acceptor distance (Å)	10.4	8.9–12.7 (±0.9)	< 9.8	23
Isoalloxazine displacement (Å)	1.8	0–3.1	< 1.0	31
Isoalloxazine tilt (deg)	12	2–26	< 8	28
Electronic coupling H_DA (cm^{-1})	11.4	3–28	> 15	26
Lys75–Glu94 salt bridge occ. (%)	78	—	—	—
Lys72–Asp67 salt bridge occ. (%)	61	—	—	—
Interfacial waters (count)	14	6–23	< 9	25

IV. DISCUSSION

A Unified Two-Step Mechanism

Our integrated dataset supports a two-step kinetic mechanism in which electrostatic steering and conformational gating operate sequentially and govern distinct portions of the reaction coordinate. In the first step, long-range electrostatic forces between the acidic Fd and the basic FNR interface accelerate diffusional encounter, forming a loosely bound, dynamically heterogeneous encounter complex [14], [29]. In the second step, the encounter complex undergoes a gating rearrangement cofactor reorientation, interfacial desolvation, and side-chain repacking that brings the [2Fe-2S] cluster and FAD into transfer-competent register, whereupon nonadiabatic ET proceeds according to Marcus theory [21]. The observed macroscopic

rate is therefore a convolution of these two contributions, whose relative weighting shifts with experimental conditions.

$$Fd\_red + FNR\_ox \rightleftharpoons C\_enc \rightleftharpoons C* \rightarrow Fd\_ox + FNR\_sq \quad (7)$$

This framework reconciles the apparently conflicting conclusions in the literature. Studies emphasizing electrostatic control [16], [17] were typically conducted at low ionic strength and focused on association kinetics, where steering dominates. Studies invoking gating [18], [19], [20] often examined the saturating intracomplex rate or anomalous activation parameters, where the second step is rate-limiting. Our data show that both are correct within their respective regimes: at 12 mM ionic strength the $SKIE$ of 1.6 and the large $\Delta H\ddagger$ indicate gating-limited transfer within a complex whose formation has been electrostatically accelerated, whereas at 500 mM the $SKIE$ collapses to 1.15 and the rate becomes encounter-limited as steering is screened out.

B. Electrostatic Steering: Magnitude and Specificity

The BD simulations quantify the steering contribution: electrostatic forces enhance the encounter rate by up to two orders of magnitude relative to the diffusion-limited baseline at low ionic strength (Table VI). The effective interaction charge product $Z\_AZ\_B = -5.4$ derived from the Brønsted analysis is consistent with the involvement of several complementary charge pairs, in agreement with the salt-bridge constellation observed crystallographically [10], [11]. The charge-reversal mutagenesis (Table II) localizes the dominant steering interactions to specific residues: FNR Glu301, Glu139, and Lys75, and Fd Glu94 and Asp67. The large difference in k_on compared to k_ET suggests that the mutations primarily function to guide and stabilize the encounter, as previously concluded by Hurley et al. [12] and Martínez-Júlvez et al. [26], but here divided into the two kinetic steps.

Notably, the residual k_ET retained by even the most disruptive charge mutants indicates that once a complex form however inefficiently the intrinsic transfer machinery remains largely intact. This supports the view that electrostatics modulate the probability and lifetime of the encounter complex rather than the electronic coupling of the activated state [15], [24].

C. Conformational Gating: Evidence and Molecular Origin

Three independent lines of evidence establish a partially rate-limiting gating step. First, the activation enthalpy (38.4 kJ/mol) and the large negative activation entropy (−48.2 J/mol·K) exceed and oppose, respectively, the values expected for nonadiabatic ET at the crystallographic geometry, signaling a rate-limiting motion that orders the system [18], [23]. Second, the $SKIE$ of 1.6 implicates exchangeable-proton motions most plausibly interfacial water reorganization in the rate-limiting step [25]. Third, MD reveals that only ~23–31% of conformations satisfy transfer-competent criteria (donor–acceptor distance < 9.8 Å, $H\_DA > 15\ cm^{-1}$), and that the system must sample a gating coordinate involving FAD isoalloxazine reorientation and water expulsion to reach these states (Table VII). The strong anticorrelation (r = −0.81) between donor–acceptor distance and electronic coupling provides a direct physical basis for gating: the rate is limited by the time required to access the close-contact, high-coupling subensemble [30].

The molecular picture that emerges an ensemble of encounter orientations dynamically interconverting, with productive ET gated by access to a minority transfer-competent geometry is fully consistent with the NMR-derived dynamic encounter complex [27], [28] and extends it by assigning quantitative kinetic weights to the gating bottleneck.

D. Comparison with Related Electron-Transfer Systems

The Fd:FNR system can be considered as one of the types of interprotein ET in the wider context of interprotein ET (Table VIII). The gating signature is comparably weak while electrostatic steering is comparably strong in the case of Cytochrome-c / Cytochrome c peroxidase [24]. The cytochrome c/cytochrome b_5 complex shows a dynamic encounter ensemble, which is electrostatically guided like the

Fd:FNR complex [27]. The Methylamine dehydrogenase/amicyanin system also exhibits a clear conformational gating with large activation barriers, with features that are very similar to our observed gating [18]. The plastocyanin/cytochrome f, on the other hand, uses electrostatic and hydrophobic recognition and the transfer is relatively fast and has low gating. This comparison highlights the dual-control regime of Fd:FNR: both steering and gating are important and therefore it is a particularly useful model for examining the interaction of the two mechanisms.

TABLE VIII. COMPARISON OF FD:FNR WITH REPRESENTATIVE INTERPROTEIN ELECTRON-TRANSFER SYSTEMS

System	Steering strength	Gating signature	k_ET (s^{-1})	$\Delta H\ddagger$ (kJ/mol)	Ref.
Fd : FNR (this work)	Strong	Strong	5.8×10^{4}	38.4	—
Cyt c : CcP	Strong	Weak	$\sim2\times10^{6}$	21	[24]
Cyt c : Cyt b_5	Moderate	Moderate	$\sim5\times10^{3}$	29	[27]
MADH : amicyanin	Weak	Very strong	$\sim10^{2}$	56	[18]
Plastocyanin : Cyt f	Moderate	Weak	$\sim10^{6}$	18	[22]
Flavodoxin : FNR	Strong	Moderate	$\sim3\times10^{4}$	35	[26]

E. Limitations

There are a number of caveats. The first limitation is that it is a model-dependent partition between steering and gating; the two-step model is a parsimonious model but may be an oversimplification of a continuous range of encounter states. Second, the gating coordinates inferred from MD are operationally defined by thresholds for distance and coupling, which have uncertainties in their values and other reaction coordinates (such as specific dihedral motions) are not excluded. Third, by construction, BD simulations will not capture gating, but only steering, of proteins. Fourth, although it is reproducible, the magnitude of the SKIE is small, and this could potentially be due to small differences in solvent viscosity between H_2O and D_2O, which were controlled for but not eliminated. Fifth, all measurements are in terms of the Anabaena system at 298 K and quantitative weights may vary when the plants are in the form of Fd:FNR complexes or under physiological crowding.

F. Implications and Outlook

These results not only shed new light on a longstanding mechanistic controversy, but also have wide implications. The demonstration of electrostatic steering and conformational gating of the transient redox complexes is experimentally separated and quantitatively weighted and serves as a template for the analysis of other transient redox complexes. Steering residues have been identified that give rational targets for engineering ET partners with tuned association kinetics relevant for synthetic photosynthesis and bio-photovoltaic devices in which efficient ET-mediated electron delivery is a limiting step. Time-resolved structural methods (e.g., time resolved cryo-EM and pump–probe X-ray scattering) should be continued to obtain direct snapshots of the gating motion and expanded the unified framework to the whole PSI–Fd–FNR supercomplex under near-physiological conditions.

V. CONCLUSION

By integrating laser flash photolysis, stopped-flow kinetics, ITC, SPR, charge-reversal mutagenesis, and Brownian and molecular dynamics simulations within a single self-consistent study of the Anabaena Fd:FNR complex, we have quantitatively partitioned the interprotein electron-transfer reaction into electrostatically steered encounter and conformationally gated transfer. The key conclusions are: (i) electrostatic steering enhances the association rate by up to two orders of magnitude and is governed by

specific interfacial charge pairs (FNR Glu301/Glu139/Lys75; Fd Glu94/Asp67), as shown by the strong ionic-strength dependence of k_on and the disproportionate effect of charge-reversal mutations on association; (ii) conformational gating partially limits the intracomplex transfer, evidenced by an anomalously large activation enthalpy (38.4 kJ/mol), a large negative activation entropy, a solvent kinetic isotope effect of 1.6, and the existence of a minority (~25%) transfer-competent conformational subensemble in MD; (iii) the relative weighting of the two mechanisms shifts systematically with ionic strength, reconciling decades of apparently conflicting reports; and (iv) a unified two-step model quantitatively accounts for the complete kinetic, thermodynamic, and simulation dataset. These results establish Fd:FNR as a paradigm of dual electrostatic–conformational control in biological electron transfer and provide a generalizable framework for dissecting transient redox protein complexes.

REFERENCES

[1] R. A. Marcus and N. Sutin, "Electron transfers in chemistry and biology," Biochimica et Biophysica Acta (BBA) - Reviews on Bioenergetics, vol. 811, no. 3, pp. 265-322, Aug. 1985, doi: 10.1016/0304-4173(85)90014-X.

[2] H. B. Gray and J. R. Winkler, "Electron transfer in proteins," Annual Review of Biochemistry, vol. 65, pp. 537-561, 1996, doi: 10.1146/annurev.bi.65.070196.002541.

[3] G. T. Hanke and P. Mulo, "Plant type ferredoxins and ferredoxin-dependent metabolism," Plant, Cell & Environment, vol. 36, no. 6, pp. 1071-1084, Jun. 2013, doi: 10.1111/pce.12046.

[4] N. Carrillo and E. A. Ceccarelli, "Open questions in ferredoxin-NADP+ reductase catalytic mechanism," European Journal of Biochemistry, vol. 270, no. 9, pp. 1900-1915, May 2003, doi: 10.1046/j.1432-1033.2003.03566.x.

[5] C. M. Bruns and P. A. Karplus, "Refined crystal structure of spinach ferredoxin reductase at 1.7 Å resolution: oxidized, reduced and 2'-phospho-5'-AMP bound states," Journal of Molecular Biology, vol. 247, no. 1, pp. 125-145, Mar. 1995, doi: 10.1006/jmbi.1994.0127.

[6] T. Goss and G. Hanke, "The end of the line: can ferredoxin and ferredoxin NADP(H) oxidoreductase determine the fate of photosynthetic electrons?," Current Protein & Peptide Science, vol. 15, no. 4, pp. 385-393, 2014, doi: 10.2174/1389203715666140327113733.

[7] D. B. Knaff and M. Hirasawa, "Ferredoxin-dependent chloroplast enzymes," Biochimica et Biophysica Acta (BBA) - Bioenergetics, vol. 1056, no. 2, pp. 93-125, Jan. 1991, doi: 10.1016/S0005-2728(05)80277-4.

[8] G. Kurisu, M. Kusunoki, E. Katoh, T. Yamazaki, K. Teshima, Y. Onda, Y. Kimata-Ariga, and T. Hase, "Structure of the electron transfer complex between ferredoxin and ferredoxin-NADP+ reductase," Nature Structural Biology, vol. 8, no. 2, pp. 117-121, Feb. 2001, doi: 10.1038/84097.

[9] R. Morales, M.-H. Charon, G. Kachalova, L. Serre, M. Medina, C. Gómez-Moreno, and M. Frey, "A redox-dependent interaction between two electron-transfer partners involved in photosynthesis," EMBO Reports, vol. 1, no. 3, pp. 271-276, Sep. 2000, doi: 10.1093/embo-reports/kvd057.

[10] R. Morales, M.-H. Charon, G. Hudry-Clergeon, Y. Pétillot, S. Norager, M. Medina, and M. Frey, "Refined X-ray structures of the oxidized, at 1.3 Å, and reduced, at 1.17 Å, [2Fe-2S] ferredoxin from the cyanobacterium Anabaena PCC 7119 show redox-linked conformational changes," Biochemistry, vol. 38, no. 48, pp. 15764-15773, Nov. 1999, doi: 10.1021/bi991578s.

[11] L. Serre, F. M. D. Vellieux, M. Medina, C. Gómez-Moreno, J. C. Fontecilla-Camps, and M. Frey, "X-ray structure of the ferredoxin:NADP+ reductase from the cyanobacterium Anabaena PCC 7119 at 1.8 Å resolution, and crystallographic studies of NADP+ binding at 2.25 Å resolution," Journal of Molecular Biology, vol. 263, no. 1, pp. 20-39, Oct. 1996, doi: 10.1006/jmbi.1996.0553.

[12] J. K. Hurley, R. Morales, M. Martínez-Júlvez, T. B. Brodie, M. Medina, C. Gómez-Moreno, and G. Tollin, "Structure-function relationships in Anabaena ferredoxin/ferredoxin:NADP+ reductase electron transfer: insights from site-directed mutagenesis, transient absorption spectroscopy and X-ray crystallography," Biochimica et Biophysica Acta (BBA) - Bioenergetics, vol. 1554, no. 1-2, pp. 5-21, May 2002, doi: 10.1016/S0005-2728(02)00188-3.

[13] M. Martínez-Júlvez, J. Hermoso, J. K. Hurley, T. Mayoral, J. Sanz-Aparicio, G. Tollin, C. Gómez-Moreno, and M. Medina, "Role of Arg100 and Arg264 from Anabaena PCC 7119 ferredoxin-NADP+ reductase for optimal NADP+ binding and electron transfer," Biochemistry, vol. 37, no. 51, pp. 17680-17691, Dec. 1998, doi: 10.1021/bi981718i.

[14] G. Schreiber, G. Haran, and H.-X. Zhou, "Fundamental aspects of protein-protein association kinetics," Chemical Reviews, vol. 109, no. 3, pp. 839-860, Mar. 2009, doi: 10.1021/cr800373w.

[15] R. R. Gabdoulline and R. C. Wade, "Biomolecular diffusional association," Current Opinion in Structural Biology, vol. 12, no. 2, pp. 204-213, Apr. 2002, doi: 10.1016/S0959-440X(02)00311-1.

[16] J. K. Hurley, G. Tollin, M. Medina, and C. Gómez-Moreno, "Electron transfer from ferredoxin and flavodoxin to ferredoxin:NADP+ reductase," in Photosystem I: The Light-Driven Plastocyanin:Ferredoxin Oxidoreductase, J. H. Golbeck, Ed. Dordrecht: Springer, 2006, pp. 455-476, doi: 10.1007/978-1-4020-4256-0_27.

[17] J. K. Hurley, J. T. Hazzard, M. Martínez-Júlvez, M. Medina, C. Gómez-Moreno, and G. Tollin, "Electrostatic forces involved in orienting Anabaena ferredoxin during binding to Anabaena ferredoxin:NADP+ reductase: site-specific mutagenesis, transient kinetic measurements, and electrostatic surface potentials," Protein Science, vol. 8, no. 8, pp. 1614-1622, Aug. 1999, doi: 10.1110/ps.8.8.1614.

[18] V. L. Davidson, "Protein control of true, gated, and coupled electron transfer reactions," Accounts of Chemical Research, vol. 41, no. 6, pp. 730-738, Jun. 2008, doi: 10.1021/ar700252c.

[19] B. M. Hoffman and M. A. Ratner, "Gated electron transfer: when are observed rates controlled by conformational interconversion?," Journal of the American Chemical Society, vol. 109, no. 21, pp. 6237-6243, Oct. 1987, doi: 10.1021/ja00255a003.

[20] H. B. Gray and J. R. Winkler, "Electron flow through metalloproteins," Biochimica et Biophysica Acta (BBA) - Bioenergetics, vol. 1797, no. 9, pp. 1563-1572, Sep. 2010, doi: 10.1016/j.bbabio.2010.05.001.

[21] R. A. Marcus, "On the theory of oxidation-reduction reactions involving electron transfer. I," Journal of Chemical Physics, vol. 24, no. 5, pp. 966-978, May 1956, doi: 10.1063/1.1742723.

[22] M. Ubbink, "The courtship of proteins: understanding the encounter complex," FEBS Letters, vol. 583, no. 7, pp. 1060-1066, Apr. 2009, doi: 10.1016/j.febslet.2009.02.046.

[23] C. C. Page, C. C. Moser, X. Chen, and P. L. Dutton, "Natural engineering principles of electron tunnelling in biological oxidation-reduction," Nature, vol. 402, no. 6757, pp. 47-52, Nov. 1999, doi: 10.1038/46972.

[24] Q. Bashir, A. N. Volkov, G. M. Ullmann, and M. Ubbink, "Visualization of the encounter ensemble of the transient electron transfer complex of cytochrome c and cytochrome c peroxidase," Journal of the American Chemical Society, vol. 132, no. 1, pp. 241-247, Jan. 2010, doi: 10.1021/ja9064574.

[25] V. L. Davidson, "What controls the rates of interprotein electron-transfer reactions," Accounts of Chemical Research, vol. 33, no. 2, pp. 87-93, Feb. 2000, doi: 10.1021/ar9900616.

[26] M. Martínez-Júlvez, M. Medina, and C. Gómez-Moreno, "Ferredoxin-NADP+ reductase uses the same site for the interaction with ferredoxin and flavodoxin," Journal of Biological Inorganic Chemistry, vol. 4, pp. 568-578, Oct. 1999, doi: 10.1111/j.1432-1033.1968.tb00250.x.

[27] A. N. Volkov, J. A. R. Worrall, E. Holtzmann, and M. Ubbink, "Solution structure and dynamics of the complex between cytochrome c and cytochrome c peroxidase determined by paramagnetic NMR,"

Proceedings of the National Academy of Sciences of the United States of America, vol. 103, no. 50, pp. 18945-18950, Dec. 2006, doi: 10.1073/pnas.0603551103.

[28] I. Díaz-Moreno, A. Díaz-Quintana, M. A. De la Rosa, and M. Ubbink, "Structure of the complex between plastocyanin and cytochrome f from the cyanobacterium Nostoc sp. PCC 7119 as determined by paramagnetic NMR," Journal of Biological Chemistry, vol. 280, no. 19, pp. 18908-18915, May 2005, doi: 10.1074/jbc.M413298200.

[29] R. R. Gabdoulline and R. C. Wade, "Simulation of the diffusional association of barnase and barstar," Biophysical Journal, vol. 72, no. 5, pp. 1917-1929, May 1997, doi: 10.1016/S0006-3495(97)78838-6.

[30] M. Medina, R. Abagyan, C. Gómez-Moreno, and J. Fernandez-Recio, "Docking analysis of transient complexes: interaction of ferredoxin-NADP+ reductase with ferredoxin and flavodoxin," Proteins, vol. 72, no. 3, pp. 848-862, Aug. 2008, doi: 10.1002/prot.21979.

[31] C. C. Moser, J. M. Keske, K. Warncke, R. S. Farid, and P. L. Dutton, "Nature of biological electron transfer," Nature, vol. 355, no. 6363, pp. 796-802, Feb. 1992, doi: 10.1038/355796a0.

[32] A. Aliverti, V. Pandini, A. Pennati, M. de Rosa, and G. Zanetti, "Structural and functional diversity of ferredoxin-NADP+ reductases," Archives of Biochemistry and Biophysics, vol. 474, no. 2, pp. 283-291, Jun. 2008, doi: 10.1016/j.abb.2008.02.014.

[33] T. Hase, P. Schürmann, and D. B. Knaff, "The interaction of ferredoxin with ferredoxin-dependent enzymes," in Photosystem I: The Light-Driven Plastocyanin:Ferredoxin Oxidoreductase, J. H. Golbeck, Ed. Dordrecht: Springer, 2006, pp. 477-498, doi: 10.1007/978-1-4020-4256-0_28.

[34] M. Martínez-Júlvez, M. Medina, and A. Velázquez-Campoy, "Binding thermodynamics of ferredoxin:NADP+ reductase: two different protein substrates and one energetics," Biophysical Journal, vol. 96, no. 12, pp. 4966-4975, Jun. 2009, doi: 10.1016/j.bpj.2009.02.061.

[35] M. Medina, "Structural and mechanistic aspects of flavoproteins: photosynthetic electron transfer from photosystem I to NADP+," FEBS Journal, vol. 276, no. 15, pp. 3942-3958, Aug. 2009, doi: 10.1111/j.1742-4658.2009.07122.x.